Modified Embedded-Atom Method Interatomic Potentials for Al-Cu, Al-Fe and Al-Ni Binary Alloys: From Room Temperature to Melting Point

Avik Mahata^a, Tanmoy Mukhopadhyay^b and Mohsen Asle Zaeem^{c*}

^a School of Engineering, Brown University, Providence, RI 02912, USA
 ^b Department of Aerospace Engineering, Indian Institute of Technology Kanpur, Kanpur, India
 ^c Department of Mechanical Engineering, Colorado School of Mines, CO 80401, USA

Abstract

Second nearest neighbor modified embedded-atom method (2NN-MEAM) interatomic potentials are developed for binary aluminum (Al) alloys applicable from room temperature to the melting point. The binary alloys studied in this work are Al-Cu, Al-Fe and Al-Ni. Sensitivity and uncertainty analyses are performed on potential parameters based on the perturbation approach. The outcome of the sensitivity analysis shows that some of the MEAM parameters interdependently influence all MEAM model outputs, allowing for the definition of an ordered calibration procedure to target specific MEAM outputs. Using these 2NN-MEAM interatomic potentials, molecular dynamics (MD) simulations are performed to calculate low and high-temperature properties, such as the formation energies of stable phases and unstable intermetallics, lattice parameters, elastic constants, thermal expansion coefficients, enthalpy of formation of solids, liquid mixing enthalpy, and liquidus temperatures at a wide range of compositions. The computed data are compared with the available first principle calculations and experimental data, showing high accuracy of the 2NN-MEAM interatomic potentials. In addition, the liquidus temperature of the Al binary alloys is compared to the phase diagrams determined by the CALPHAD method.

Keywords: Interatomic potentials; binary aluminum alloys; melting; molecular dynamics.

*Corresponding author; email: <u>zaeem@mines.edu</u> (M. Asle Zaeem)

1

1. Introduction

To study different aspects of solidification of metallic materials, several computational methods have been developed and applied in different time and length scales. These studies are based on first principle calculation/density functional theory (DFT) [1], molecular dynamics (MD) [2, 3], Monte Carlo (MC) [4], phase-field [5, 6], front tracking (FT) model [7], extended finite element method (FEM) [8, 9], and some others. Each of these methods have their own advantages and shortcomings, mostly related to their length and time scales, accuracy or efficiency. Solidification begins at the atomistic realm at the interior part of the liquid, then the crystalline nuclei grow to nano and micro scale sizes before the solidification is completed. High temperature DFT based studies (also called ab initio MD) can be used to study some melting properties such as the free energies, enthalpies, heat of melting during the change of phase [10, 11], but they are limited to very small time and length scales, which prevent them from directly observing the evolution of solidification nano/microstructures. The DFT based calculation of such melting properties at very small scale are extremely computationally intensive, which makes it challenging to extend it any practical melting studies. MC simulations are also performed in very small length scales, whereas FT or FEM methods for solidification are applied for much larger scales, nonetheless they are mostly qualitative studies [12, 13]. Phase-field is a popular method to study solidification at the micro scale, but in order to have quantitative results, most of its model parameters need to be determined by other methods, like MD simulations [14].

MD has gained popularity in nucleation-solidification research due to its flexibility in the length scale, which can span from a few thousand atoms to multibillion atom systems. In one of our previous studies [3] and also in various other MD works [15-17], the critical nucleus size, nucleation temperature, and incubation time for different metals were shown to be in good agreement with those from experimental studies and/or classical nucleation theory (CNT). However, the accuracy of MD simulations significantly depends on the interatomic potentials [18, 19], and suitable interatomic potentials are needed to study melting and solidification.

The initial MD studies of solidification based on pair potentials, such as Lennard-Jones potential [20-22] and hard sphere model [23, 24], were not accurate enough. Later, many body interatomic potential such as, embedded atom method (EAM) [25, 26] and Finnis–Sinclair (FS) [27] were developed which enhanced the capability and accuracy of MD simulations at low temperatures, however, both EAM and FS cannot predict the thermal properties and high

temperature properties accurately. The modified embedded-atom method (MEAM) was introduced to include the directionality of bonding in the EAM formalism for covalent materials in [28, 29]. Previously it was shown that the MEAM formalism successfully reproduces the low temperature physical properties of face-centered cubic (fcc) [30, 31], body-centered cubic (bcc) [39], hexagonal close-packed (hcp) [29] and diamond cubic [32] crystal structures. Recently, the MEAM formalism has been extended to predict low temperature physical properties of binary [32, 33] and ternary alloys [34, 35]. In our recent studies of solid-liquid coexistence of Al, Cu, Ni [36], Fe [36, 37] we showed that it is possible to modify the MEAM potential parameters to predict low temperature, high temperature and melting properties of these metallic elements more accurately than any other interatomic potentials. Also in a study by Ryu and Cai [38], the MEAM formalism was shown to be more accurate in predicting the thermal properties if several single element metals compared to other many body interatomic potentials such as FS, EAM and Stillinger-Weber (SW) potential [39].

There is a demand for developing more accurate interatomic potentials for alloy systems, especially those capable of predicting properties in a wide range of temperatures. To the best our knowledge, there are no such interatomic potentials for Al binary alloys, which are some of the most theologically important alloys for light weighting. In this study, we focused on Al-Cu, Al-Fe and Al-Ni alloys. 2NN-MEAM interatomic potentials are developed and MD simulations are completed to calculate low and high temperature properties of these alloys in a wide range of compositions. In previous studies, the thermal properties and melting temperature for Al, Cu, Ni and Fe elements were calculated by 2NN-MEAM MD simulations and verified by experimental data [36, 40, 41], and we use this single element 2NN-MEAM interatomic potentials in this work. First, the interatomic potential for each binary alloy is parameterized for the available stable compounds. During the optimization of potential parameters, we have also quantified the sensitivity of output properties with respect to each parameter. Then, the next stage of parameterization is done while verifying the solid and liquid mixing enthalpy of the alloys, thermal expansion, and high temperature lattice parameters. After the interatomic potential shows good accuracy in determining some of the low and high temperature properties, we calculate the solidliquid coexistence properties at different compositions. Finally, we determine the formation energies of intermetallic and other theoretical structures, which can be crucial for performing studies on precipitations in Al alloys.

2. Computational Methodology

2.1 MEAM interatomic potential

The MEAM interatomic potential introduced by Baskes [28] is very successful in predicting the properties in single or multi component metallic materials. Second nearest neighbors (2NN) were taken into consideration to further improve the MEAM formulism by Lee and Baskes [42], which also resulted in better predictions of solid-liquid coexistence properties. Details of the 2NN-MEAM potential can be found in the previously published papers by Baskes and co-workers [42-44], and are briefly reviewed in this paper. Within the MEAM approach, the total energy, *E*, for a system of atoms is approximated by the embedding energy and screening factor as shown below,

$$E = \sum_{i} F(\rho_{i}) + \frac{1}{2} \sum_{j \neq i} S_{ij} \phi_{ij} (r_{ij}).$$
 (1)

The term $\sum_i F(\rho_i)$ in Eqn. (1) is the embedding energy, which can be interpreted as the energy to insert an atom at site i into the background electron density ρ_i . The background electron density is computed by combining several partial electron density terms with weighting factors of $t^{(h)}$ (h=0-3) corresponding to s, p, d, and f orbital symmetries, and for convenience $t^{(0)}$ is taken as 1. Each partial electron density is a function of the atomic configuration of the system and the atomic electron density. The atomic electron densities at a distance r are computed as:

$$\rho^{a(h)}(r) = \rho_0 \exp\left[-\beta^{(h)} \left(\frac{r}{r^e} - 1\right)\right],\tag{2}$$

where ρ_0 is the atomic electron density scaling factor, r^e is the nearest-neighbor distance in the equilibrium reference structure, and the decay lengths, $\beta^{(h)}$, are element-dependent adjustable parameters. The embedding energy function has the following form:

$$F(\overline{\rho_i}) = \begin{cases} AE^c \overline{\rho_i} \ln(\overline{\rho_i}) & \text{for } \overline{\rho_i} \ge 0 \\ AE^c \overline{\rho_i} & \text{for } \overline{\rho_i} < 0 \end{cases}$$
(3)

where A is an adjustable dimensionless parameter of order unity, and E^c is the cohesive energy of a reference structure.

The second term on the right-hand side of Eqn. (1) includes the screening function, S_{ij} , and the pair potential interaction function, $\phi_{ij}(r_{ij})$, between atoms i and j separated by distance r_{ij} . The value of the pair interaction function is not obtained by using a predetermined functional form, but instead, it is evaluated from the known values of total energy and the embedding function of an atom in the equilibrium reference structure. The total energy per atom in the equilibrium reference structure, $E^u(R)$, is obtained as a function of the nearest-neighbor distance, R, and the scaled distance, R, and is calculated using the modified zero-temperature universal Rose–Vinet equation of state [45] given by:

$$E^{u}(R) = -E^{c} \left(1 + a^{*} \delta \frac{r^{e}}{R} a^{*3} \right) e^{-a^{*}}, \tag{4}$$

where δ is an adjustable parameter. The scaled distance is related to the nearest neighbor distance by:

$$a^* = \alpha^0 \left(\frac{R}{r^e} - 1 \right), \tag{5}$$

where α^0 is a parameter related to the bulk modulus, cohesive energy, and the equilibrium atomic volume in the reference state. The pair interaction is evaluated from the known values of total energy per atom and the embedding energy as a function of the nearest-neighbor distance.

In practice, the range of interactions is limited by using either a screening function or a cut-off procedure. When screening is used, both the atomic electron densities and the pair potential interactions between atoms i and j are multiplied by a screening function, S_{ij} , which has values in the range between 0 and 1 [46]. The two extreme values of $S_{ij} = 0$ and 1 mean the interaction between the atoms i and j is fully-screened and non-screened, respectively. In the original MEAM potential only the first nearest-neighbor interactions were considered by employing strong screening functions. The 2NN-MEAM potential partially considers 2NN interactions by adjusting the screening parameters (C_{\min}, C_{\max}) so that the many-body screening becomes less severe.

Fig. 1 shows a graphical depiction of ellipses used in the definition of contributing term of the screening factor of atoms i and j by the neighboring atom k for face-centered cubic (fcc) and body-centered cubic (bcc) structures; the origin is set midway between i and j. One can consider an ellipse passing through atoms i, j, and k with the minor axis on the line connecting atoms i and j.

Thus, using the length of the minor axis as r_{ij} equal to the distance between atom i and j, the equation of this ellipse is given by:

$$x^2 + \frac{y^2}{C} = \left(\frac{1}{2}r_{ij}\right)^2,\tag{6}$$

where parameter C controls the elongation of the ellipse in the y-direction and is given by:

$$C = \frac{2(X_{ij} + X_{kj}) - (X_{ik} + X_{kj}) - 1}{1 - (X_{ik} - X_{kj})^2} ,$$
 (7)

where $X_{ik} = (r_{ik} / r_{ij})^2$ and $X_{kj} = (r_{kj} / r_{ij})^2$. The corresponding values of C for the perfect fcc and bcc crystal structures are 1 and 2, respectively. The blue and red lines in Fig. 1 are the ellipses for C values corresponding to perfect BCC and FCC crystal structures.

In 2NN-MEAM potential, the contributing terms, S_{ijk} , are determined by two parameters C_{\min} and C_{\max} . When the ellipse passing through atoms i,j, and k is located outside the ellipse defined by C_{\max} , it means that the atom k does not screen the interaction between atoms i and j and S_{ikj} will be equal to 1. If the ellipse passing through atoms i,j, and k is located inside the region delimited by the ellipse defined by C_{\min} , it means that the atom k fully screens the interaction between atoms i and j and, S_{ikj} will be equal to 0. When the ellipse passing through atoms i,j, and k is located between the two ellipses defined by C_{\max} and C_{\min} , S_{ijk} will vary smoothly between 0 and 1.

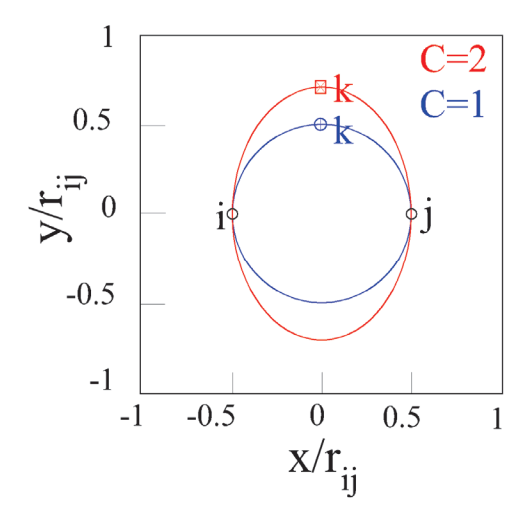


Fig. 1 Graphical depiction of the ellipses used in the definition of contributing term of the screening factor of atoms i and j by the neighboring atom k for fcc and bcc structures.

2.2 Calibration and optimization of MEAM potential parameters

We have recently developed 2NN-MEAM potential parameters for Al, Cu, Ni [36], and Fe [37, 47] single elements that can predict the low and high temperature properties. The optimized parameters for single elements are shown in Table 1. In general, the parameter-property relationship is complicated and one cannot easily relate one property to one parameter in the potential. However, some parameters can be connected to specific properties; for example, α^0 has a higher influence on elastic properties, and $t^{(1-3)}$ significantly affect the high temperature melting properties. The low temperature properties, such as the formation energies, lattice constants and elastic constants, were predicted exceptionally accurately. These interatomic potentials predict the melting points of Al, Cu, Ni and Fe to be 925 K, 1358 K, 1742 K and 1807 K, respectively (Table 2), which all are very close to the experimental data. In addition, the other melting properties, such as the latent heat, expansion in melting, specific heat and solid-liquid interfacial free energies, remain within 5-9% error margin compared to experimental data [36, 37, 40, 41, 47]. We also validated the liquid structure factor and radial distribution function at the melting points for all the single elements, and it showed excellent agreement with data available from various experiments. Overall, the MD simulations with the MEAM parameters in Table 1 predict excellent solid-liquid coexistence properties of these metallic systems [36, 37], and have been also used to study crystal nucleation [3], evolution of solidification defects [48], and directional solidification [49], therefore we use the same potential parameters for single elements.

Table 1. 2NN-MEAM parameters for binary Al alloys are shown. $E^c(eV)$ (Eqn. 3) is the cohesive energy; $R_0(\mathring{A})$ is the nearest neighbor distance in the equilibrium reference structure; α^0 is the exponential decay factor for the UEOS of Rose et al. [50]; Asub (A) is the electron density scaling factor for the embedding function; $\beta^{(0-3)}$ are the exponential decay factors for the atomic electron densities; $t^{(1-3)}$ are the weighting parameters for the atomic electron densities; and C_{\min} and C_{\max} are the screening parameters. C_{\max} is taken 2.8 for all the cases.

Element	$E^{c}(eV)$	$R_0(\mathring{A})$	A	α^0	$\beta^{(0)}$	$\beta^{(1)}$	$\beta^{(2)}$	$\beta^{(3)}$	t ⁽¹⁾	t ⁽²⁾	t ⁽³⁾	C_{\min}
Al [36]	3.36	2.86	1.16	4.61	3.20	2.60	6.0	2.60	3.05	0.51	7.75	0.49
Cu [36]	3.54	2.56	0.99	5.20	3.83	2.20	6.0	2.20	2.72	3.04	0.85	1.21
Ni [36]	4.45	2.49	0.99	5.08	2.56	1.50	6.0	1.50	3.10	1.80	2.20	0.81
Fe [37]	4.90	2.47	0.57	5.03	3.67	1.00	1.00	1.00	2.90	1.00	-8.7	0.16

Table 2. Calculated melting temperature $T_m(K)$, and latent heat of fusion ΔH_f (kJ/mol) for pure Al, Cu, Ni, and Fe using the 2NN-MEAM potentials [36, 37], and the corresponding data from experiments [51]. Uncertainties are for 95% confidence intervals.

	Al		Cu		Ni		Fe	
Property	Experiment	2NN MEAM	Experiment	2NN MEAM	Experiment	2NN MEAM	Experiment	2NN MEAM
T_m	933.5	924.9	1357.8	1319.6	1728.0	1741.6	1811	1807
ΔH_f	10.71	11.50	13.26	14.21	17.48	22.17	13.8	13.0

Since we have verified and used the single element interatomic potentials for various mechanical and solidification properties, these MEAM potentials for single elements can be used to develop the potential parameters for alloy systems. In MEAM, E^c , R_0 , α^0 and the attraction-repulsion term describe the material properties. So, the experimental data available from the literature can be fitted by altering the E^c , R_0 , α and the attraction-repulsion parameters for the alloys. Instead of E^c , we fit the heat of formation ΔH for an alloy, which is the difference of the cohesive energy of the alloy to the average of each of the element in the alloy. The alloy phases are most likely to form at the lowest heat of formation which occurs at T=0 K. In the MEAM calculation, we define the heat of formation as:

$$\Delta H = \frac{E_{tot}(N_x + N_y) - N_x \varepsilon_x - N_y \varepsilon_y}{N_x + N_y}.$$
 (8)

 E_{tot} is the total energy of the simulation cell, N_x and N_y are the numbers of type-X and type-Y atoms in the cell, and ε_x and ε_y are the total energies per atom for type X and type Y in their ground-state bulk structures, respectively. For all the binary alloys, we utilized the experimental data for B2 (Al-Fe, Al-Ni) or other stable phases (Al₂Cu for Al-Cu) for the initial parameterization. Then, we studied the formation enthalpy by changing the alloying content from 0 to 100 atomic (at.) %. If the results did not replicate the experimental results then we modified the ΔH , R_0 , α^0 , C_{\min} , C_{\max} and the attraction-repulsion parameters, and recalculate the elastic properties and

formation energies. In the iterative process to optimize the potential parameters, the priority was given to accurate predictions of the heat of formation, and solidus and liquidus temperatures.

For the initial fitting to B1 and B2 structures, we utilized MEAM Parameter Calibration (MPCv4) tool [52, 53], and the MD simulations were performed in LAMMPS [54]. MPCv4 does optimization of the different MEAM parameters in a sequence starting with calibration to fcc/bcc/hcp energy versus lattice parameters, then calibration to bulk modulus and elastic constants, and the final calibration for vacancy formation energy and stacking fault energy [53]. In practice, we provide a calibration range for the different fcc/bcc/hcp and stacking fault energies for the Al alloys to MPCv4, and then it optimizes the MEAM parameters according to the range of calibration. Due to large number of parameters, there may be some uncertainties in the parameter values. This can be addressed by introducing Pareto optimality through recent multi-objective evolutionary algorithms that allow simultaneous optimization of a number of physical properties [55].

The overall uncertainty in MEAM parameters provided by MPCv4 is often very low [56]. In general, uncertainties for the energies (fcc/bcc/hcp) are all very small (<1%). The largest uncertainties is reported for the elastic moduli (C₄₄ approximately 10%). A parameter dominated in terms of model sensitivity while A and $\beta^{(0-3)}$ (See Table 1 for the parameters) dominated in terms of uncertainty percentage contribution. The sensitivity analysis revealed that the coefficient of the embedding function related to the background electron density, A, was the most influential parameter [56]. In case of Al, Fe, Cu and Mg, the MEAM parameters were fully optimized for both low and high temperature properties of the single element, so the sets of calibrated MEAM parameters fit the low temperature properties such as formation energy, elastic properties very accurately for different alloy structures.

Some MEAM parameters fail in predicting the high temperature and solid-liquid coexistence properties. MPCv4 produces a restart file for each of calibrations and we can recalibrate with newer parameters for properties at different temperatures. We used the two-phase solid—liquid coexistence to determine the exact liquidus line for the binary components. The exact liquidus line in the phase diagram was calculated by simultaneously equilibrating the solid and liquid phases in a simulation box. The methods have been discussed in detail in our previous works [36, 40]. The model used for single elements have only one single phase, however for alloys, the

composition (at. % of the alloying element) is used to form both the solid and the liquid. To calculate the solid–liquid interface stiffness a slab of two-phase coexisting solid–liquid is used. The slab has a thickness of b, a width of W and a length of L (normal to the solid–liquid interface direction), where b << W. The two-phase solid–liquid coexisting slab is equilibrated at the melting point using the method explained in the preceding section. This slab consists of $m \times n \times l$ lattice cells, where m, n and l are the number of periodic lattice cells along the width, thickness and normal directions, respectively. The equilibrations steps involve NPT and NVT at the liquidus temperature. In the final step, we equilibrated without any temperature control by NPH simulation. The final temperatures predicted utilizing the NPH simulations are our estimated liquidus temperature. Table 3 shows the final MEAM potential parameters for all the binary interactions.

Table 3. The MEAM potential parameters for element pairs. Heat of formation, $\Delta H_{B1/B2}^{XY}(eV)$, where B1(NaCl) or B2(AlFe) is the reference structure with the type-X and type-Y elements relative to the energies of elemental X and Y in their equilibrium reference state, $r_e^{XY}(\mathring{A})$ is their equilibrium nearest neighbor distance, α^{XY} is the exponential decay factor for the universal energy, and C_{\min} and C_{\max} are screening parameters (C^{XYX} denotes type-Y element between two elements). C_{\max} for all the cases is 2.8.

X	Y	$\Delta H_{B1/B2}^{XY}(eV)$	$R_0^{XY}(\mathring{A})$	α^{XY}	$C_{ m min}^{\mathit{XYX}}$	C_{\min}^{YXY}	C_{\min}^{XXY}	C_{\min}^{XYY}
Al	Cu	0.20	2.53	4.65	0.50	1.00	0.00	0.90
Al	Fe	0.27	2.49	5.50	2.00	2.00	0.00	2.00
Al	Ni	0.25	2.75	5.58	2.00	2.00	2.00	1.60

2.3 Uncertainty quantification and sensitivity analysis

MEAM potentials generally have around 14 different primary potential parameters that can impact the material properties [28]. From the application of MEAM parameters in predicting materials behavior, we understand that not all the parameters significantly change the outcome of simulations or noticeably affect the properties [41]. For single element cases, α , β , t, C_{\min} are the most dominant parameters; we have fitted those parameters in our previous studies for Al, Cu, Ni, Fe and Mg [36, 37, 40, 47]. For binary alloys, we focus on the primary mixing parameters such as α^{XY} , C_{\min}^{XYY} , C_{\min}^{XYY} , C_{\min}^{XYY} and C_{\min}^{XYY} . To perform the uncertainty and sensitivity analyses for our MEAM parameters, the potential parameters are the input parameters and we consider per-

atom energy (*E*) and the elastic parameters (*C*₄₄, *C*₁₁ and bulk modulus) as the output parameters. It is noted that the set of output parameters N_0^{All} (*E*, *C*₄₄, *C*₁₁ and bulk modulus) is treated as the function of five input parameters (α^{XY} , C_{\min}^{XYX} , C_{\min}^{XYY} , C_{\min}^{XXY} and C_{\min}^{XYY}). We consider a small degree of source-uncertainty around the mean values of the input parameters ($\mu_{\overline{s}} = \{\mu_{\overline{s}_1}, \mu_{\overline{s}_2}, \dots, \mu_{\overline{s}_m}\}$, where m = 5), which results in the uncertainty of output parameters N_0^{All} . Thus, the output parameters can be expressed by implementing the Taylor series expansion as [56-58]

$$N_{0}^{All}(\overline{s}) = N_{0}^{All}(\boldsymbol{\mu}_{\overline{s}}) + \sum_{j=1}^{m} \left[\frac{\partial N_{0}^{All}(\overline{s})}{\partial \overline{s}_{j}} \right|_{\overline{s} = \boldsymbol{\mu}_{\overline{s}}} \left[(\overline{s}_{j} - \boldsymbol{\mu}_{\overline{s}_{j}}) \right]$$

$$+ \frac{1}{2} \sum_{j=1}^{m} \sum_{q=1}^{m} \left[\frac{\partial N_{0}^{All}(\overline{s})}{\partial \overline{s}_{j}} \right|_{\overline{s} = \boldsymbol{\mu}_{\overline{s}}} \left[(\overline{s}_{j} - \boldsymbol{\mu}_{\overline{s}_{j}}) (\overline{s}_{q} - \boldsymbol{\mu}_{\overline{s}_{q}}) + \mathbf{H}(\overline{s}) \right]$$

$$(9)$$

where $\mu_{\overline{s}_j}$ denotes the mean of the j^{th} random input parameter; $\mathbf{H}(\overline{s})$ denotes higher-order terms of the Taylor series expansion for the uncertainties \overline{s} . Implementing the first-order perturbation theory (FOPT) by neglecting the second-order and higher-order terms in the above equation, the mean $\mu^{(I)}$ and variance $\sigma^{2(I)}$ of the stochastic output parameters N_0^{All} can be explicitly estimated as

$$\mu_{N_{\alpha}^{All}(\overline{s})}^{(I)} = N_0^{All} \left(\mathbf{\mu}_{\overline{s}} \right) , \tag{10}$$

$$\sigma_{N_0^{All}(\overline{s})}^{2(I)} = \sum_{j=1}^{m} \sum_{q=1}^{m} \left[\frac{\partial N_0^{All}(\overline{s})}{\partial \overline{s}_j} \bigg|_{\overline{s} = \mathbf{\mu}_{\overline{s}}} \right] \cdot \left[\frac{\partial N_0^{All}(\overline{s})}{\partial \overline{s}_q} \bigg|_{\overline{s} = \mathbf{\mu}_{\overline{s}}} \right] \cdot \text{cov}(\overline{s}_j, \overline{s}_q), \tag{11}$$

where $\operatorname{cov}\left(\overline{s}_{j}, \overline{s}_{q}\right)$ is the covariance between the j^{th} and the q^{th} input parameters such that $\operatorname{cov}\left(\overline{s}_{j}, \overline{s}_{q}\right) = 0$ if \overline{s}_{j} and \overline{s}_{q} are uncorrelated, and $\operatorname{cov}\left(\overline{s}_{j}, \overline{s}_{q}\right) = \sigma_{\overline{s}_{j}}^{2} = \sigma_{\overline{s}_{q}}^{2}$ if j = q. Here, assuming negligible correlation among the input parameters, the uncertainty of the output parameters in

terms of standard deviation $(\sigma_{N_0^{All}(\bar{s})}^{(I)})$ can be obtained using one-factor-at-a-time first-order perturbation method (2m+1) function evaluations) based on central difference approximation as

$$\frac{\partial N_0^{All}}{\partial \overline{s}_j} = \frac{N_0^{All} (\mu_{\overline{s}_j} + p_j) - N_0^{All} (\mu_{\overline{s}_j} - p_j)}{2p_j} \ . \tag{12}$$

In the above expression, p_i represents the perturbation size for the j^{th} input parameter.

Based on the mean and standard deviation of the output parameters N_0^{All} , the sensitivity of j^{th} input parameter (ζ_j) can be calculated as

$$\zeta_{j} = \frac{\left(\frac{\sigma_{N_{0}^{All}(\bar{s})}^{(I)}}{\mu_{N_{0}^{All}(\bar{s})}^{(I)}}\right)_{j}}{\sum_{j=1}^{m} \left(\frac{\sigma_{N_{0}^{All}(\bar{s})}^{(I)}}{\mu_{N_{0}^{All}(\bar{s})}^{(I)}}\right)_{j}},$$
(13)

where $\sum_{j=1}^{m} \zeta_{j} = 1$. In the above expression, the quantities in the numerator and denominator represent the coefficient of variation in N_{0}^{All} due to uncertainty in only the j^{th} input parameter and summation of the coefficient variations for all the input parameters, respectively.

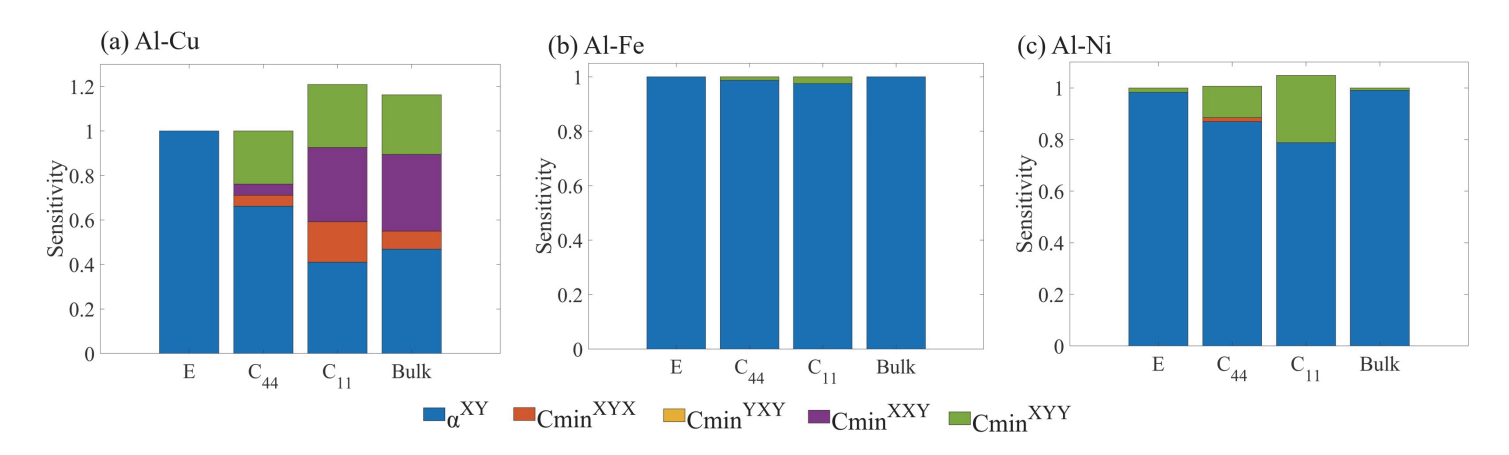


Fig. 2. Sensitivity analysis of output properties with respect to each of the input MEAM parameters are shown for (a) Al-Cu, (b) Al-Fe and (c) Al-Ni.

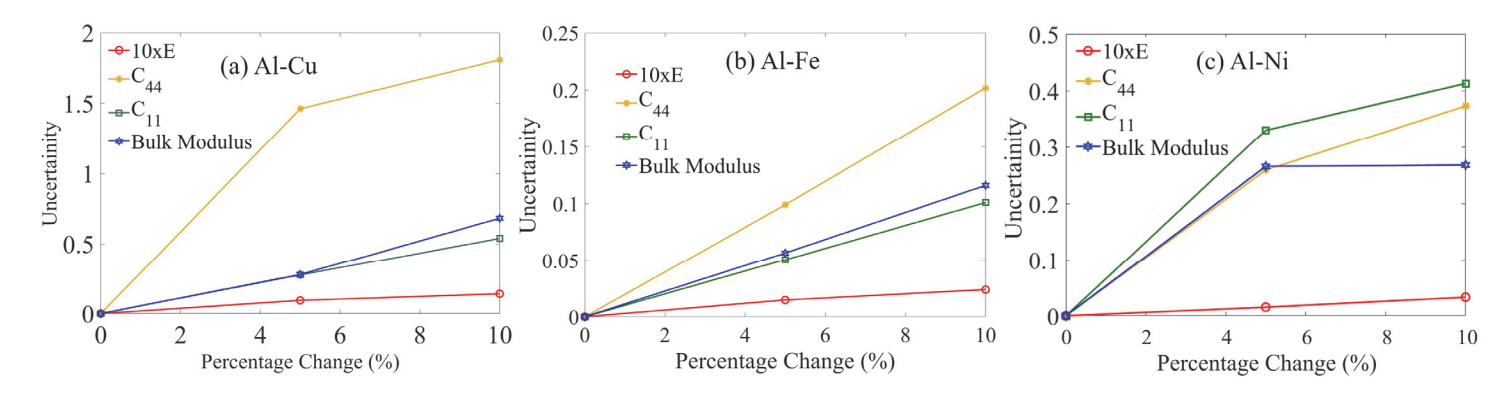


Fig. 3. Uncertainty for the increasing change in the input MEAM parameters are shown for (a) AlCu, (b) Al-Fe and (c) Al-Ni.

Based on first order perturbation theory, as presented above, we have numerically quantified the uncertainty and sensitivity associated with the output parameters and input parameters, respectively. We have shown the sensitivity of the parameters α^{XY} , C_{\min}^{XYX} , C_{\min}^{XYY} , C_{\min}^{XYY} , and C_{\min}^{XYY} on the four output properties (E, C_{44} , C_{11} and bulk modulus) considering Al-Cu, Al-Fe and Al-Ni alloys (refer to Figure 2). It can be noted that α^{XY} is the predominantly sensitive parameter for all the output properties and all the alloys under consideration. This observation is in good agreement with previous studies on similar sensitivity analysis [52, 53].

We have quantified the compound effect of uncertainty considering deferent degree of variation p_j (i.e. percentage change) in all the input parameters simultaneously. Numerical results of uncertainty in terms of the standard deviation of the output parameters (E, C_{44} , C_{11} and bulk modulus) normalized with respect to the corresponding nominal values are presented for Al-Cu, Al-Fe and Al-Ni alloys (refer to Figure 3). A general trend is noticed that the uncertainty in all the output quantities increases with the increase in percentage variations of the input parameters. However, the input-output relationships are different for each of the output parameters depending on the material under consideration, as evident from the nature of the curves.

3. Results and Discussions

3.1 Al-Cu binary alloys

Al₂Cu-θ and Al₂Cu-θ' phases are very stable and well researched Al-Cu compounds both experimentally [59] and computationally [60, 61]. First, we study the 2NN-MEAM interatomic

potential of Al-Cu to investigate its accuracy in prediction of experimental properties of Al₂Cu phases. Table 4 shows the formation energies, elastic properties, interfacial energies, surface energies for both Al₂Cu precipitates. The formation energy, ΔE_f , of all the compounds $Al_m M_n (M=Cu,Ni,Fe)$ in Al binary alloys is defined relative to the cohesive energy of pure Al and the formation energy of the alloying element as,

$$\Delta E_f = \frac{1}{n+m} \left[E(Al_n M_m) - n E_{fcc}(Al) - m E_{bcc/fcc}(M) \right]. \tag{14}$$

Where, $E(Al_nM_m)$ is the total energy of the simulation with m+n number of atoms, and $E_{fcc}(Al)/E_{bcc/fcc}(M)$ is the cohesive energy shown in Table 1. For some compounds, the experimental data are not available for all different properties, so we use first principle data for comparison.

Table 4. The formation energy, elastic properties, and surface and interfacial energies for $Al_2Cu-\theta$ and θ ' phases predicted by 2NN-MEAM MD simulations compared with literature data. The superscripts a, b and c denote data from experiments, first principle/DFT calculations, or previous MD simulations, respectively.

	Al ₂ Cu-θ (C16)	Al ₂ Cu-θ' (C1)		
Properties	Experiments/First Principle/MD	MEAM MD	Experiments/First Principle	MEAM MD
Lattice	6.064 ^a [62], 6.067 ^a [63], 5.96 ^b [64], 6.067 ^b [65], 6.049 ^b [66], 5.935-5996 ^c [67]	6.027	5.725a [59], 5.68 ^b [64], 5.668 ^c [67]	5.704
Parameters (Å)	4.874 ^a [62], 4.877 ^a [63], 4.77 ^b [64], 4.8777 ^b [65], 4.891 ^b [66], 4.908-4.914 ^c [67]	4.895	5.812ª [59]	-
Formation Energy (eV/atom)	-0.135 ^a [62], -0.139 ^a [63], - 0.184 ^b [68], -0.169 ^b [65], -0.190 ^c [67], 0.180 ^c [69]	-0.187	-0.199b [70], -0.203- 0.74° [67]	-0.161
Bulk Modulus (GPa)	113.4 ^a [71] 99.4 ^b [65], 147.6 ^c [67]	113.11	117 ^b [68], 135.9-199.2 ^c [67]	121.845
C ₁₁ (GPa)	186.20 ^a [71], 150.3 ^b [65], 199.3 ^c [67]	166.23	190 ^b [70], 192.8-310.5 ^c [67]	188.724
C_{12} (GPa)	71.5 ^a [71], 86.1 ^b [65], 98.2 ^c [67]	86.33	80 ^b [72]	88.352
C ₄₄ (GPa)	29.2^a [66], 29.4^b [65], $59.7-78.6^c$ [67]	40.0	90 ^b [72]	77.312
Surface Energies (Jm ⁻²)				
$\gamma_{\rm s}$ (100)	1.266,1.294° [67]	1.335	1.093-1.524° [67]	1.951
r _s (110)	1.463,1.522° [67]	1.605	1.043-1.465° [67]	1.396
$\gamma_{\rm s}$ (111)	-	1.113	1.768-1.371° [67]	1.695
Interfacial				
Energy	-	-	0.615-0.694° [69]	0.632
Al-Al ₂ Cu (Jm ⁻²)				

The interatomic potential is also tested for other Al-Cu intermetallic compounds (Table 5). The MEAM potential accurately predicts the energies for B1 and the other Cu rich composition

such as, L1₂, A15 and D0₂₂. However, MEAM slightly underestimates or overestimates the formation energy for the Al rich compound such as, Al₃Cu, Al₃Cu₂ and AlCu. compared to previous DFT studies. These intermetallics were also studied by the ADP (angular-dependent potential) interatomic potential [67], and it follows a similar pattern of overestimating the formation energy for Al rich compounds.

To verify the applicability of the interatomic potential at high temperatures, first, the thermal linear expansion coefficient of Al₂Cu, Al₄Cu₉, AlCu and AlCu₃ is verified. As shown in Fig. 4(a), 2NN-MEAM MD simulations reproduced the experimental results. In Fig. 4(b) and (c) the enthalpy of formation of solid and liquid alloys is shown. To determine the liquid enthalpy, liquid Al-Cu alloys were equilibrated at a very high temperature to produce a homogenous liquid. Then the temperature of the liquid was brought down to the desired temperatures such as 1373-1773 K (Fig. 4(c)), and the system was equilibrated for 1000 ps to record the formation energies. A similar system of pure Al and Cu were also equilibrated at the same temperature after producing the liquid at a higher temperature, then energies of liquid Al and Cu were used as the reference. The time steps in MD simulations are limited to picosecond or nanosecond scale. If the system can be equilibrated for a longer time, the formation energies may become even closer to the experimental data.

Table 5. Formation energies of different possible Al-Cu compounds compared with first-principle data and previous MD simulations. The unit for formation energies is eV/atom.

Formula	Structure	MEAM (this work)	Expt/DFT/MD
Al ₃ Cu	L12	-0.18	-0.284 [33]
Al_3Cu_2	D519	-0.299	-0.164 [72]
AlCu	B2	-0.435	-0.198 [33], -0.195 [73]
AlCu	B1	-0.205	-0.190 [33]
AlCu	"40"(NbP)	-0.0159	-0.191 [73]
AlCu	B32	-0.009	0.024 [73]
Al ₄ Cu ₉	D83	-0.136	-0.215 [66]
AlCu ₃	L12	-0.179	-0.182 [67]
AlCu ₃	A15	-0.141	-0.136 [33]
AlCu ₃	D022	-0.185	-0.185 [72]

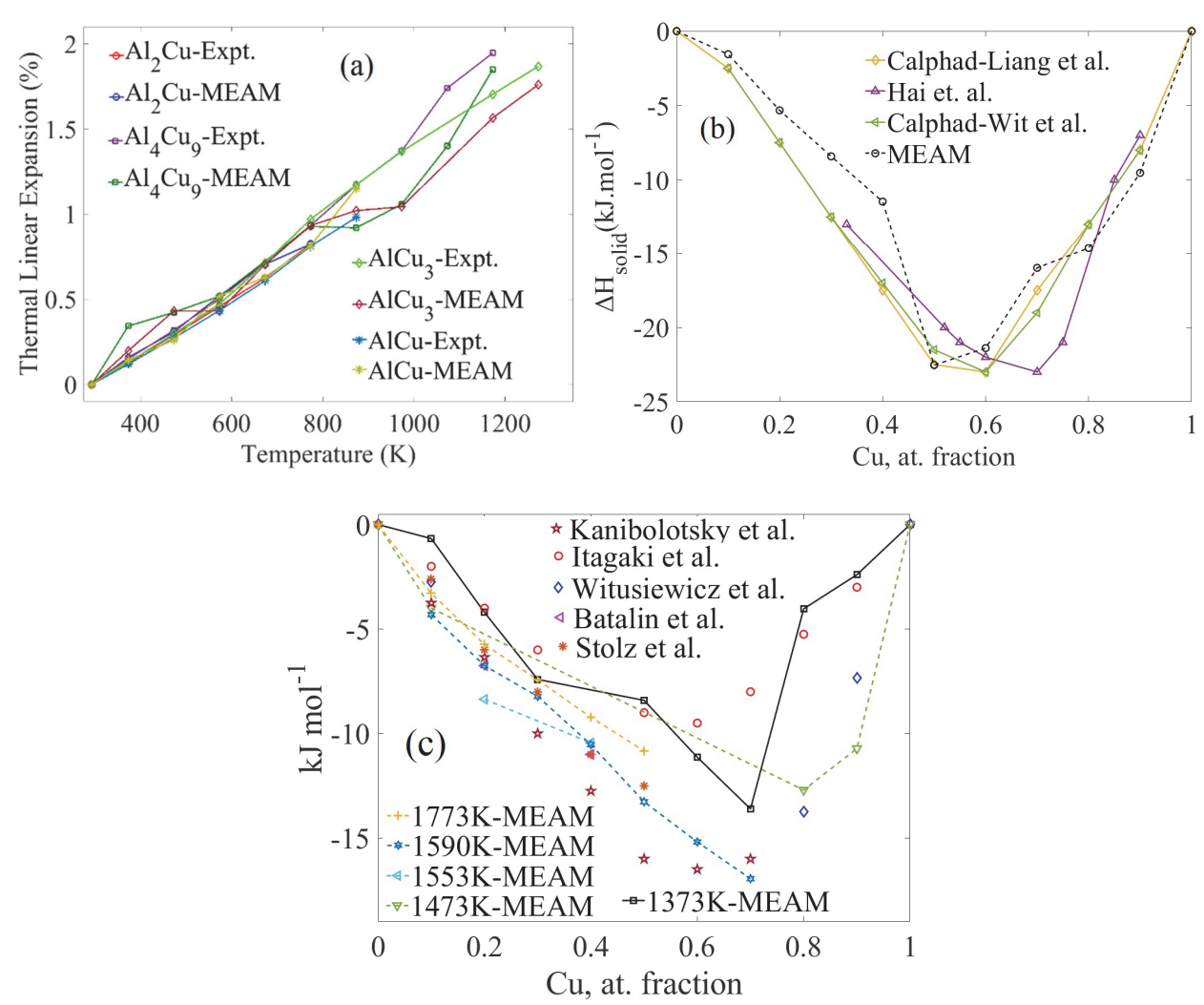


Fig. 4. (a) Calculated thermal linear expansion for different Al-Cu compounds and intermetallics such as Al₂Cu, Al₄Cu₉, AlCu and AlCu₃. The experimental data of thermal expansion is obtained from Touloukian et. al. [74]. (b) The enthalpy of formation of solid phases is compared with experimental data at 773K from Liang et al. [75], Witusiewicz et al. [76], and Hair et. al. [77]. (c) Liquid mixing enthalpy for Al-Cu versus Cu content. The experimental values for different temperature between 1373-1773 K are taken from the literature [78-83].

Unlike single element metallic systems, we can refer the melting temperature as solid-liquid coexistence temperature or simply solidus/liquidus temperature. For validating the liquidus temperatures, data from the phase diagrams of all the binary alloys are used. It is necessary to validate the solidus-liquidus temperature for each alloy to ensure the accuracy of interatomic potentials close to melting and at different compositions. The solid-liquid coexistence temperature is calculated by simultaneously equilibrating the solid and liquid phases in a simulation box. A simulation box consisting of $m \times n \times l$ periodic solid cells are equilibrated at an estimated solidus/

liquidus temperature of each alloy [47], where the *l* direction is normal to the solid–liquid interface and longer than the other two directions. Then, the central half of the simulation box is melted at a high temperature by running a dynamics simulation using a canonical ensemble (NVT) with a Nose–Hoover thermostat [84, 85], while holding the other half fixed. The melted half of the simulation box is equilibrated at the estimated melting point using an isothermal-isobaric (NPT) ensemble for 0.5 ns, while the box size in the normal direction is allowed to relax, and still holding the other solid half fixed. The entire simulation box is allowed to relax in the normal direction for 1 ns using an NPT ensemble at the estimated coexistence temperature (to minimize the pressure in all directions). Finally, the refined value of the liquidus temperature is calculated using an isenthalpic ensemble (NPH) simulation lasting for ~10 ns, while the size of the box in the normal direction is allowed to relax (to minimize the normal pressure). The whole process is repeated using the calculated refined temperature instead of the estimated coexistence temperature until convergence is achieved.

Detailed experimental or theoretical solidus and liquidus line for changing amount of Cu in Al in Al-Cu alloy can be found in the work by Predel et al. [86]. In Table 6 the solid-liquid coexistence is calculated using the current 2NN-MEAM potential, and the predicted liquidus temperatures are almost similar to the temperatures reported in the phase diagram. At 100% Al and the eutectic point, the solidus and liquidus lines are expressed by a single point.

Table 6. The liquidus temperature from the experimental phase diagram is compared with the prediction of 2NN-MEAM results. The * is the eutectic point.

Al-Cu Composition (Al-at. % of Cu)	Liquidus Temperature (K) (Expt.) [86]	2NN- MEAM MD (K)
Al	933.5	925
Al-10% Cu	873.0	868±5
Al-15% Cu*	821.2	821±5
Al-25% Cu	853.0	849±10
Al-50% Cu	1148.0	1170±15
Al-75% Cu	1300	1310±8
Cu	1357	1320

3.2 Al-Ni binary alloys

Similar to Al-Cu, Al-Ni has the L12 and B2 crystal structures available naturally. The lattice parameters, formation energy and bulk modulus for Al-Ni B2 structures are initially utilized to parametrize the potential. Then, MEAM parameters are modified to also reproduce the formation energies of other phases. As shown in Table 7, MEAM reproduces the experimental and first principle results very accurate. The interface energy for γ -Ni and γ '-AlNi3 is also available from Silva et al. [87], which we calculated utilizing a larger supercell (50 x 25 x 25 unit cells). The calculation of interfacial energy involves two steps. First, we calculate the total energy of the supercell with full atomic relaxations, $E_{total}(a,b,c)$ with a, b, and c representing the relaxed lattice parameters of the supercell and the interface is coincident with b and c. Then in the second step, utilizing a supercell with the same size as step 1, calculate the total energies for the single γ -Ni and γ '-AlNi3 phase using the fixed lattice parameters b and c (periodic boundary condition) derived in previous step but allowing a to be relaxed (free boundary condition). Their total energies are denoted by E_{γ} and $E_{\gamma'}$, respectively. Then the interfacial energy can be calculated as,

$$\sigma = \left\{ E_{total}(a,b,c) - \frac{1}{2} \left[E_{\gamma} + E_{\gamma'} \right] \right\} / 2s, \qquad (15)$$

where *s* represents the area of the interface.

In addition, we studied the Al-Ni intermetallic compounds for their formation energies. The formation energies calculated by 2NN-MEAM for most intermetallics have a small margin of errors compared to literature data (Table 8). There are also different formation energies were reported in different publications [78, 96, 100] because the computed values of formation energies depend on the crystallographic structures used in the work. We relaxed our structures before calculating the formation energies and as it works well with naturally existing Al-Ni compounds as shown in Table 7, we expect the predictions from MEAM potentials are consistent with the other structures.

Table 7. The formation energy, elastic properties, surface and interfacial energies for AlNi₃-L1₂ and AlNi-B2 phases predicted from 2NN-MEAM MD simulations are compared with literature data. The superscripts a, b and c denote data from experiments, first principle/DFT calculations, or previous MD simulations, respectively.

	AlNi ₃ (L1	AlNi (B2)		
Properties	Experiments/First Principle	2NN- MEAM MD	Experiments/First Principle/MD	2NN- MEAM MD
Lattice Parameters (Å)	3.567 ^a [88]	3.566	2.886 ^a [88], 2.866 ^c [87]	2.867
Formation Energy (eV/atom)	-0.436 ^a [89], - 0.436 ^c [87],	-0.437	-0.604-0.69 ^a [90-92], -0.50- 0.83 ^b [93-96], -0.71.5 ^c [87, 97],	-0.600
Bulk Modulus (GPa)	177ª [98]	179	158ª [99]	160.26
C_{11} (GPa)	230 ^a [98]	254	199° [99]	192.92
C_{12} (GPa)	150° [98]	142.70	137 ^a [99]	143.94
C ₄₄ (GPa)	131 ^a [98]	115	116 ^a [99]	127.58
Interfacial Energy (Jm ⁻²) γ -Ni and γ'- AlNi ₃	0.0396° [87]	0.043	-	-

Table 8. Formation energies of different possible Al-Ni compounds compared with first-principle data and previous MD simulation. The superscripts a, b and c denote data from experiments, first principle/DFT calculations, or previous MD simulations, respectively. The unit for formation energies is eV/atom.

Formula	Structure	2NN-MEAM MD	Expt./DFT/MD
Al ₃ Ni	DO ₃	-0.375	-0.393 ^a [78], -0.439 ^b [100], -0.236 ^b [96], -0.330 ^c [101]
AISINI	DO_{20}	-0.603	-0.019 ^b [96]
	L1 ₂	-0.232	-0.250 ^b [96], -0.401 ^b [102]
Al ₄ Ni ₃	I112	-0.478	-0.683 ^b [100]
Al_3Ni_2	D5 ₁₃	-0.209	-0.499 ^b [96]
AlNi	B32	-0.215	-0.485 ^b [96], -0.351 ^c [101]
AINI	$L1_0$	-0.486	-0.572 ^b [96]
Al ₂ Ni ₃	P4	-0.534	-0.509 ^b [102]
Al ₃ Ni ₅	C16	-0.170	-0.63 ^b [100], -0.583 ^b [103]
A ING.	DO_3	-0.223	-0.262 ^b [96]
AlNi ₃	DO ₂₂	-0.589	0.949 ^b [96]

The thermal properties of Al-Ni alloys are shown in Fig. 5. The thermal linear expansion shows a very good agreement with the experimental data (Fig. 5(a)). The mixing enthalpy of solid alloys at 980 and 1100 K also closely follows the experimental results presented in Fig. 5(b). As the Ni content increase in Al-Ni alloys, the small difference in the energy in the solid solution can be attributed to the strain energy that can result in comparatively higher formation energy. In liquid, the strain energy doesn't play any role, and the predicted liquid mixing enthalpy remains very close to the experimental results at different compositions (Fig. 5(c)).

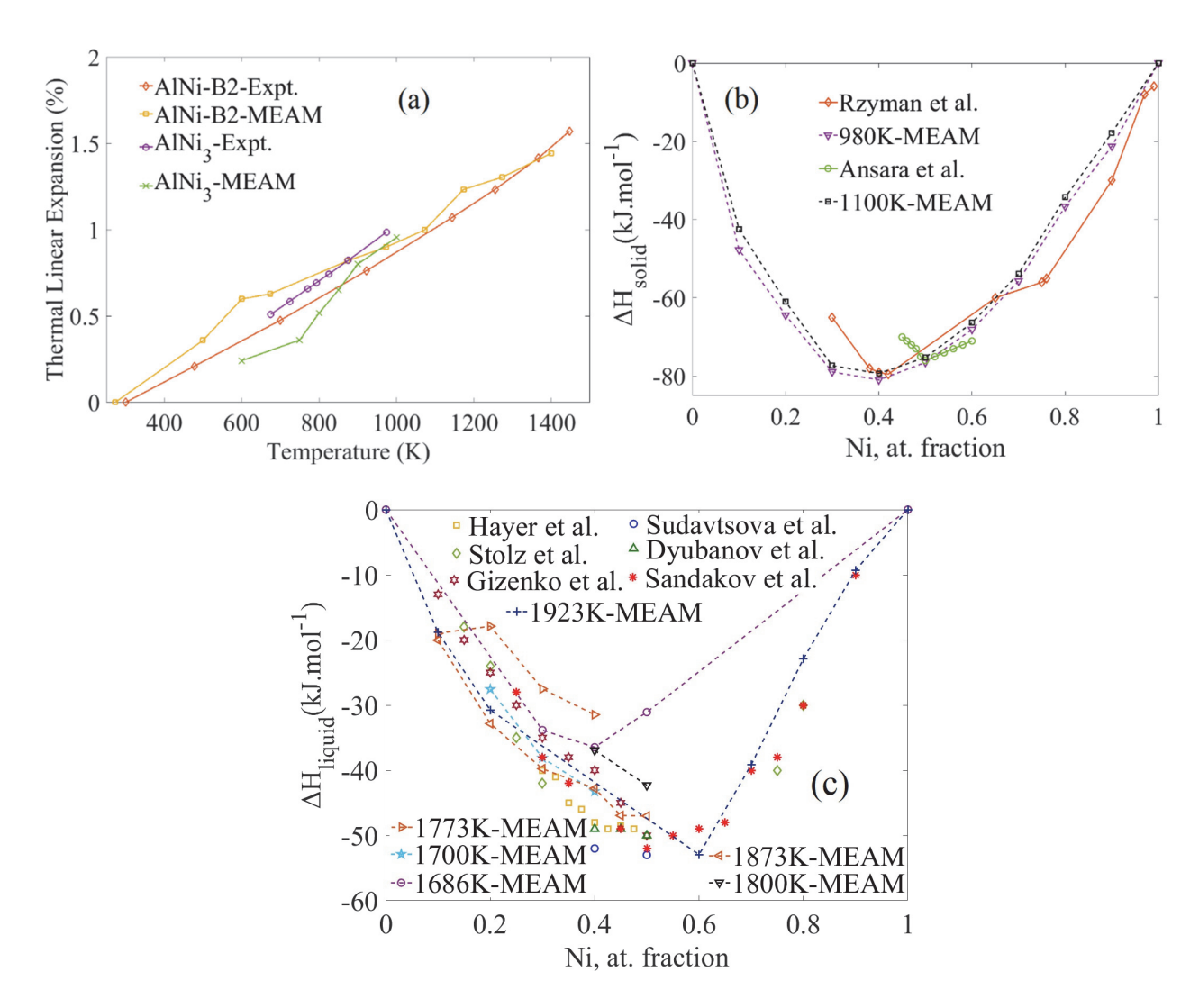


Fig. 5. (a) Calculated thermal linear expansion for different Al-Ni compounds and intermetallics such as AlNi and AlNi₃. The experimental data of thermal expansion is obtained from Touloukian et al. [74]. (b) The enthalpy of formation of solid phases is compared with experimental data at 980 and 1100 K, Rzyman et al. [104], Ansara et al. [105] and Hcnig et al. [106]. (c) Liquid mixing enthalpy for Al-Ni with increasing Ni content. The experimental values for different temperatures between 1686 K and 1923 K are taken from various CALPHAD or experimental data [90, 93, 105, 107-109].

Finally, the liquidus temperature is verified for different Ni content (Table 9). At lower Ni content, the liquidus temperature remains close to the phase diagram data, however, as the Ni content increases, the liquidus temperature is slightly overestimated. This may have happened because the MEAM interatomic potential predicts the melting temperature for Cu 14 K higher than experimental values where as it predicts 8.5 K lower melting point for Al. Regardless, the deviation experimental result remains leas than 5% for all of compositions.

Table 9. The liquidus temperature from the experimental phase diagram is compared with the prediction of 2NN-MEAM results. * is the eutectic point.

Al-Ni Composition (Al-at. % of Ni)	Liquidus Temperature (K) (Expt.) [86]	2NN- MEAM MD (K)
Al-0%Ni	933.5	925
Al-2% Ni*	917	922±2
Al-10% Ni	1050	1074±2
Al-20% Ni	1150	1180±10
Al-50% Ni	1949	2039±50
Al-75% Ni	1624	1689±20
Al-90% Ni	1700	1720±8
Al-100% Ni	1728	1742

3.3 Al-Fe binary alloys

For Al-Fe binary system, we first fit the parameters for Al-Fe B2 structure, which naturally exists and has been extensively studied experimentally for its physical properties [110-112]. Once the potential parameters are fitted for the B2 Al-Fe formation energies and elastic properties, the properties of D0₃ and L1₂ are considered for further modification of parameters. The potential parameters are compromised accordingly for fitting all the formation energies. As shown in Table 10, the formation energies and lattice parameters are reproduced with less than 1% error compared with literature data. Among the elastic properties, only C44 is underestimated, and this is in the expense of fitting all the formation energies and elastic properties and also the high temperature melting properties.

Table 10. The formation energy, elastic properties, surface and interfacial energies for FeAl-B2, Fe₃Al-DO₃ and Fe₃Al-L1₂ phases predicted from 2NN-MEAM MD are compared with litreature data. The superscripts a, b and c denote data from experiments, first principle/DFT calculations, or previous MD simulations, respectively.

	AlFe (B2)		Al Fe ₃ (DO ₃))	Al Fe ₃ (L1 ₂))
Properties	Experiments/First Principle/MD	MEAM MD	Experiments/First Principle/MD	MEAM MD	Experiments/First Principle/MD	MEAM MD
Lattice Parameters (Å)	2.90 ^a [88], 2.91 ^b [113], 2.919 ^c [114-116]	2.901	2.89 ^a [88], 2.88-2.895 ^b [115-119]	2.882	3.645-3.669 ^b [116, 117, 120]	3.600
Formation Energy (eV/atom)	-0.250-0.280 ^a [78, 91, 117, 121], -0.311- 0.420 ^b [66, 103, 122, 123], -0.342 ^c [33], 0.298 ^c [114]	-0.267	-0.202 ^a [78], -0.321 ^a [124], -0.200-0.230 ^b [33, 66, 103, 117, 125], -0.206 ^c [114]	-0.223	-0.187-0.222 ^b [66, 103, 117, 122]	-0.177
Bulk Modulus (GPa)	136 ^a [98], 155-172 ^b [116-118], 124.6 ^c [114]	135.676	144.1 ^a [98], 151-174 ^b [116-118], 148.9 ^c [114], 137.5 ^c [33]	146.00	143-185 ^b [116, 117, 120], 166.3 ^c [33], 149.6 ^c [114], 139.5 ^c [33]	145.293
C ₁₁ (GPa)	181.1 ^a [98], 143-185 ^b [116-118, 120], 124.6 ^c [114]	172.641	171.0 ^a [98], 164 ^b [116], 159.2 ^b [118], 222.5 ^c [114]	212.08	184 ^b [116], 174.3 ^c [114]	181.289
C ₁₂ (GPa)	113.7° [98], 105.0- 130.0° [116, 118, 126], 152.7° [114], 145.3° [33]	117.193	130.6 ^a [98], 127- 1327.5 ^b [117, 118] 121.1 ^c [114]	113.00	145 ^b [116], 137.2 ^c [114]	127.295
C ₄₄ (GPa)	127.1 ^a [98], 138.8 ^b [33], 78.0 ^c [114], 111.7 ^c [33]	88.00	131.7 ^a [98], 140 ^b [33], 109.1 ^c [114], 129 ^c [33]	97.50	160 ^b [116], 125.1 ^b [33], 96.9 ^c [33], 76.0 ^c [114]	72.00

The formation energies for various intermetallic and imaginary structures of Al-Fe system are calculated by utilizing the 2NN-MEAM potentials, and similar to other alloys, the results in the literature for Al-Fe alloys have large differences. However, in most of these cases, the

formation energy remains close to the one predicted by first principle calculations, therefore it is possible some of these phases form during solidification of Al-Fe alloys.

Table 11. Formation energies of different possible Al-Fe compounds compared with first-principle data and previous MD simulation. The superscripts a, b and c denote experimental, first principle/DFT of previous MD simulation data, respectively. The unit for formation energies is eV/atom.

Formula	Structure	2NN-MEAM MD	Expt./DFT/MD
Al ₆ Fe	C8	-0.172	-0.196 ^b [102]
Al ₉ Fe ₂	P32	0.114	-0.236 ^b [102]
	A15	0.481	-0.161 ^b [33], 0.321 ^c [33]
Al ₃ Fe	L12	0.428	-0.122 ^b [33] -0.105 [103], -0.049 ^c [33]
	DO_3	0.223	-0.025 ^b [33] , 0.266 ^c [33]
Al ₂ Fe	C11 _b	0.280	-0.371 b, -0.42 b [103], 0.106c[33]
	C1	-0.051	-72 ^b [33], -76 ^c [33]
Al ₁₂ Fe ₇	P4	0.099	-0.313 [102]
Al ₈ Fe ₅	I52	-0.272	-0.283 [102]
AlFe	hp6	0.973	0.807 [102]
AlFe2	C15	0.042	-0.099[102] - 0.115[33], - 0.060[103], 0.925°[33]
AlFe ₄	B24	-0.025	-0.060 [102]

After fitting the potential parameters to reproduce the low temperature properties, the thermal expansion, solid-solution enthalpy and liquid mixing enthalpy of Al-Fe alloys are studied (Fig. 6). The thermodynamic properties (enthalpy of formation and enthalpy of mixing) are reproduced well within the scattering range of experimental or first principles data. We also

compare the results of the 2NN-MEAM MD simulations to previous MEAM MFD simulations for Al-Fe alloys by Lee et al. [114].

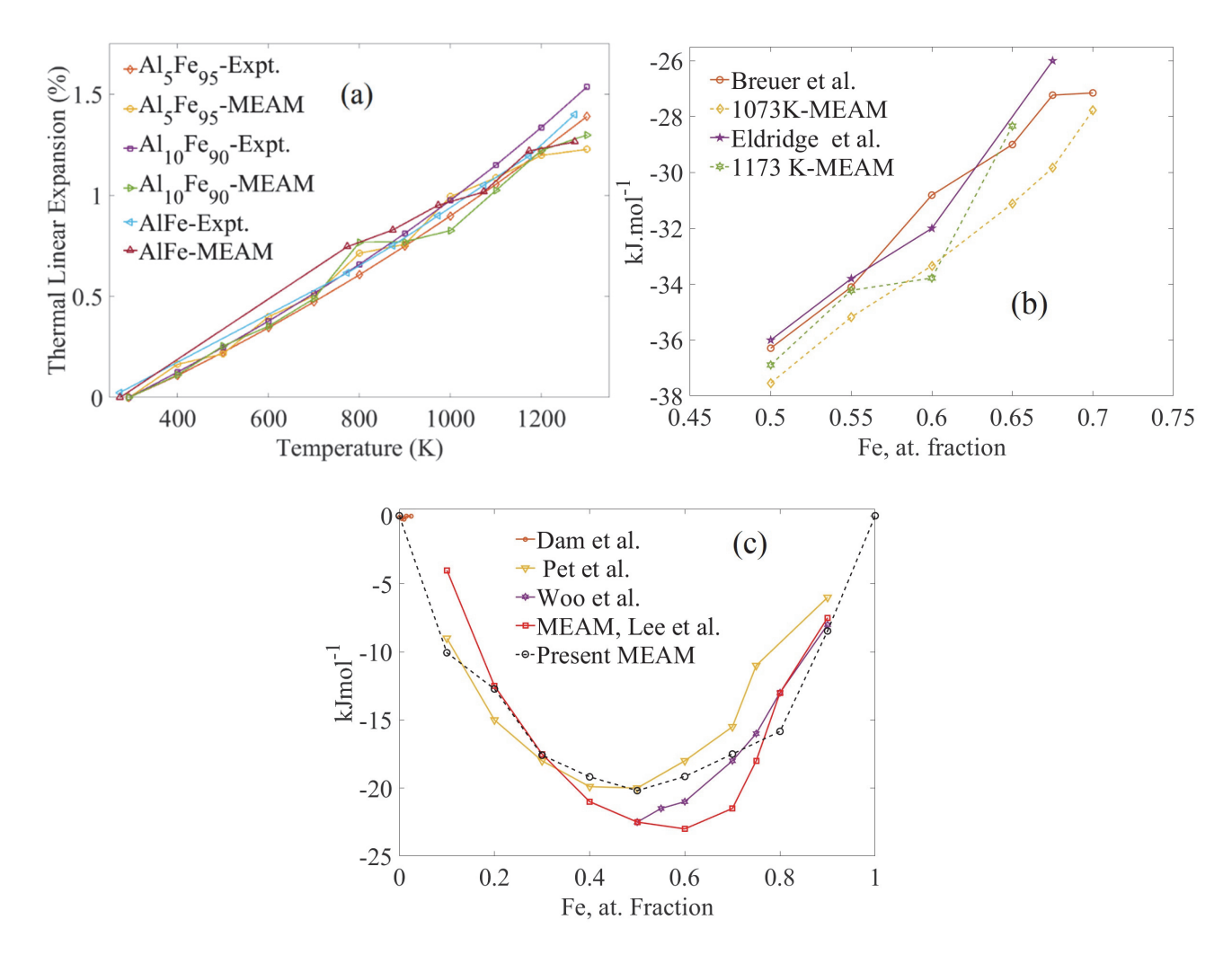


Fig. 6. (a) Calculated thermal linear expansion for different Fe content in Al-Fe alloy. The experimental data of thermal expansion is obtained from Touloukian et. al. [74]. (b) The enthalpy of formation of solid phases is compared with experimental data at 1073 and 1173 K from Breuer et al. [127] and Eldridge et al. (c) Liquid mixing enthalpy for Al-Fe with increasing Fe content. The experimental values for liquid Al-Fe alloys has been taken from various MD data from Lee et. al. [114] or experimental data from Elliott and Woolley [128], Petrushevsky et. al. [129] and Dannöhl et al. [130].

After 2NN-MEAM is fitted for the thermal properties, the high temperature solid-liquid coexistence temperatures are calculated for different at.% of Fe. The predictions from MD simulations are very close to the experimental data [86]. Fe–Al binary system is characterized by a large solubility of Al (up to 50 at. % Al) in the body-centered cubic (bcc) solid solution. Due to

mostly single phase bcc or fcc dominates at a particular at. % of Fe in Al-Fe and as a result the two-phase solid-liquid temperature coexistence remains very close to the experimental data.

Table 12. The liquidus temperature from the experimental phase diagram is compared with the prediction of 2NN-MEAM MD simulations.

Al-Fe Composition (Al-at. % of Fe)	Liquidus Temperature (K) (Expt.) [86]	2NN- MEAM MD (K)
Al-0%Fe	933.5	925
Al-10% Fe	1273	1302±10
Al-25% Fe	1435	1432±10
Al-50% Fe	1650	1663±15
Al-80% Fe	1790	1780±15
Al-90% Fe	1805	1805±5
Al-100% Fe	1809	1807

4. Conclusion

We developed 2NN-MEAM interatomic potentials of binary Al alloys for both low and high-temperature applications. Sensitivity and uncertainty analyses are performed on the MEAM potential parameters based on the perturbation approach. The outcome of the sensitivity analysis shows that some of the MEAM parameters interdependently influence all MEAM model outputs to varying degrees. The numerical results show that among the primary mixing parameters, α^{XY} , which is the exponential decay factor for the universal energy, is by far the most dominant parameter for determining the material property output from the potential. A general trend is noticed that the uncertainty in all the output quantities increases with the increase in percentage variations of the input parameters. However, the input-output relationships are different for each of the output parameters depending on the material under consideration, as quantified in this study. The final 2NN-MEAM potentials for Al-Cu, Al-Fe and Al-Ni reproduced the experimental

formation energies of various stable phases and intermetallic. These binary potentials also predicted the melting properties and solid-liquid coexistence temperatures very close to the phase diagrams of these Al-binary alloys. Other physical properties, such as interfacial energies between different metallic phases, surface energies, thermal expansion coefficient, solid-solid and solid-liquid mixing enthalpies were in reasonable agreement with experimental data, first principle calculations and/or thermodynamic calculations. The solid-liquid coexistence temperatures (liquidus temperature) for the three binary Al alloys at different compositions were calculated by 2NN-MEAM MD simulations with less than 5% error margin compared with the experimental data. As one of the most promising aspects of these 2NN-MEAM potentials, the eutectic temperatures of Al-Cu at 15% Cu and Al-Ni at 2% Ni were also predicted with high accuracy, which are 821±5 K and 922±2 K, respectively. Therefore these potentials can reproduce the phase separation and other precipitates at the eutectic points. The interatomic potential developed in this work is one step toward designing Al based multicomponent metallic alloys by predicting their physical properties.

Acknowledgments

This study was supported by the National Science Foundation under grant number NSF-CMMI 2031800. The authors are grateful for computer time allocation provided by the Extreme Science and Engineering Discovery Environment (XSEDE), award number TG-DMR140008.

Author Contribution

Avik Mahata: Conceptualization, Methodology, Software, Formal analysis, Writing-Original draft preparation. **Tanmoy Mukhopadhyay**: Methodology, Software, Formal analysis, Writing-Original draft preparation. **Mohsen Asle Zaeem**: Supervision, Conceptualization, Methodology, Formal analysis, Writing-Original draft preparation, Funding Acquisition.

Data Availability

All necessary data generated or analyzed during this study are included in this published article and the supplementary materials, and other auxiliary data are available from the corresponding author on reasonable request.

Competing Interests

The authors declare no competing interests.

Supplementary Materials

The potential files, MEAM and library files, are included as supplementary materials.

References

- [1] Y.A. Chang, S. Chen, F. Zhang, X. Yan, F. Xie, R. Schmid-Fetzer, W.A. Oates, Phase diagram calculation: past, present and future, Progress in Materials Science 49(3-4) (2004) 313-345.
- [2] M.H. Grabow, G.H. Gilmer, A.F. Bakker, Molecular dynamics studies of silicon solidification and melting, MRS Online Proceedings Library Archive 141 (1988).
- [3] A. Mahata, M. Asle Zaeem, M.I. Baskes, Understanding homogeneous nucleation in solidification of aluminum by molecular dynamics simulations, Modelling and Simulation in Materials Science and Engineering 26(2) (2018) 025007.
- [4] A. Das, S. Ji, Z. Fan, Morphological development of solidification structures under forced fluid flow: a Monte-Carlo simulation, Acta Materialia 50(18) (2002) 4571-4585.
- [5] W.J. Boettinger, J.A. Warren, C. Beckermann, A. Karma, Phase-field simulation of solidification, Annual review of materials research 32(1) (2002) 163-194.
- [6] A. Karma, Phase-field formulation for quantitative modeling of alloy solidification, Physical Review Letters 87(11) (2001) 115701.
- [7] M. Zhu, C. Hong, D. Stefanescu, Y. Chang, Computational modeling of microstructure evolution in solidification of aluminum alloys, Metallurgical and Materials Transactions B 38(4) (2007) 517-524.
- [8] J. Chessa, P. Smolinski, T. Belytschko, The extended finite element method (XFEM) for solidification problems, International Journal for Numerical Methods in Engineering 53(8) (2002) 1959-1977.
- [9] A. Dalhuijsen, A. Segal, Comparison of finite element techniques for solidification problems, International journal for numerical methods in engineering 23(10) (1986) 1807-1829.
- [10] M.J. Mehl, J.E. Osburn, D.A. Papaconstantopoulos, B.M. Klein, Structural properties of ordered high-melting-temperature intermetallic alloys from first-principles total-energy calculations, Physical Review B 41(15) (1990) 10311-10323.
- [11] S.-L. Wang, Y. Pan, Insight into the structures, melting points, and mechanical properties of NbSi2 from first-principles calculations, Journal of the American Ceramic Society 102(8) (2019) 4822-4834.
- [12] X. Sun, P. Dong, Analysis of aluminum resistance spot welding processes using coupled finite element procedures, WELDING JOURNAL-NEW YORK- 79(8) (2000) 215-S.
- [13] H.-C. Tseng, C. Hung, C.-C. Huang, An analysis of the formability of aluminum/copper clad metals with different thicknesses by the finite element method and experiment, The International Journal of Advanced Manufacturing Technology 49(9) (2010) 1029-1036.
- [14] S. Kavousi, B.R. Novak, M.I. Baskes, M. Asle Zaeem, D. Moldovan, Modified embedded-atom method potential for high-temperature crystal-melt properties of Ti–Ni alloys and its application to phase field

- simulation of solidification, Modelling and Simulation in Materials Science and Engineering 28(1) (2019) 015006.
- [15] M. Horsch, J. Vrabec, H. Hasse, Modification of the classical nucleation theory based on molecular simulation data for surface tension, critical nucleus size, and nucleation rate, Physical Review E 78(1) (2008) 011603.
- [16] X.-M. Bai, M. Li, Test of classical nucleation theory via molecular-dynamics simulation, The Journal of chemical physics 122(22) (2005) 224510.
- [17] G.C. Sosso, J. Chen, S.J. Cox, M. Fitzner, P. Pedevilla, A. Zen, A. Michaelides, Crystal nucleation in liquids: Open questions and future challenges in molecular dynamics simulations, Chemical reviews 116(12) (2016) 7078-7116.
- [18] K. Kadau, T.C. Germann, P.S. Lomdahl, Molecular dynamics comes of age: 320 billion atom simulation on BlueGene/L, International Journal of Modern Physics C 17(12) (2006) 1755-1761.
- [19] Y. Shibuta, S. Sakane, E. Miyoshi, S. Okita, T. Takaki, M. Ohno, Heterogeneity in homogeneous nucleation from billion-atom molecular dynamics simulation of solidification of pure metal, Nature Communications 8(1) (2017) 10.
- [20] M.J. Mandell, J.P. McTague, A. Rahman, Crystal nucleation in a three-dimensional Lennard-Jones system: A molecular dynamics study, The Journal of Chemical Physics 64(9) (1976) 3699-3702.
- [21] S.-N. Luo, A. Strachan, D.C. Swift, Nonequilibrium melting and crystallization of a model Lennard-Jones system, The Journal of Chemical Physics 120(24) (2004) 11640-11649.
- [22] M. Maddox, K. Gubbins, A molecular simulation study of freezing/melting phenomena for Lennard-Jones methane in cylindrical nanoscale pores, The Journal of chemical physics 107(22) (1997) 9659-9667.
- [23] I. Maxwell, A. Hellawell, A simple model for grain refinement during solidification, Acta Metallurgica 23(2) (1975) 229-237.
- [24] L. Gránásy, T. Pusztai, Diffuse interface analysis of crystal nucleation in hard-sphere liquid, The Journal of Chemical Physics 117(22) (2002) 10121-10124.
- [25] M.S. Daw, M.I. Baskes, Embedded-atom method: Derivation and application to impurities, surfaces, and other defects in metals, Physical Review B 29(12) (1984) 6443.
- [26] S. Foiles, M. Baskes, M.S. Daw, Embedded-atom-method functions for the fcc metals Cu, Ag, Au, Ni, Pd, Pt, and their alloys, Physical review B 33(12) (1986) 7983.
- [27] A. Sutton, J. Chen, Long-range finnis—sinclair potentials, Philosophical Magazine Letters 61(3) (1990) 139-146.
- [28] M.I. Baskes, Modified embedded-atom potentials for cubic materials and impurities, Physical Review B 46(5) (1992) 2727-2742.
- [29] M. Baskes, R. Johnson, Modified embedded atom potentials for HCP metals, Modelling and Simulation in Materials Science and Engineering 2(1) (1994) 147.
- [30] B.-J. Lee, J.-H. Shim, M. Baskes, Semiempirical atomic potentials for the fcc metals Cu, Ag, Au, Ni, Pd, Pt, Al, and Pb based on first and second nearest-neighbor modified embedded atom method, Physical Review B 68(14) (2003) 144112.
- [31] S.M. Valone, M.I. Baskes, M. Stan, T.E. Mitchell, A.C. Lawson, K.E. Sickafus, Simulations of low energy cascades in fcc Pu metal at 300 K and constant volume, Journal of nuclear materials 324(1) (2004) 41-51.
- [32] Y.-M. Kim, B.-J. Lee, Modified embedded-atom method interatomic potentials for the Ti–C and Ti–N binary systems, Acta materialia 56(14) (2008) 3481-3489.
- [33] B. Jelinek, S. Groh, M.F. Horstemeyer, J. Houze, S.-G. Kim, G.J. Wagner, A. Moitra, M.I. Baskes, Modified embedded atom method potential for Al, Si, Mg, Cu, and Fe alloys, Physical Review B 85(24) (2012) 245102.
- [34] B.-J. Lee, W.-S. Ko, H.-K. Kim, E.-H. Kim, The modified embedded-atom method interatomic potentials and recent progress in atomistic simulations, Calphad 34(4) (2010) 510-522.

- [35] D.E. Dickel, M.I. Baskes, I. Aslam, C.D. Barrett, New interatomic potential for Mg–Al–Zn alloys with specific application to dilute Mg-based alloys, Modelling and Simulation in Materials Science and Engineering 26(4) (2018) 045010.
- [36] E. Asadi, M. Asle Zaeem, S. Nouranian, M.I. Baskes, Two-phase solid–liquid coexistence of Ni, Cu, and Al by molecular dynamics simulations using the modified embedded-atom method, Acta Materialia 86 (2015) 169-181.
- [37] E. Asadi, M. Asle Zaeem, S. Nouranian, M.I. Baskes, Quantitative modeling of the equilibration of two-phase solid-liquid Fe by atomistic simulations on diffusive time scales, Physical Review B 91(2) (2015) 024105.
- [38] S. Ryu, W. Cai, Comparison of thermal properties predicted by interatomic potential models, Modelling and Simulation in Materials Science and Engineering 16(8) (2008) 085005.
- [39] F.H. Stillinger, T.A. Weber, Computer simulation of local order in condensed phases of silicon, Physical review B 31(8) (1985) 5262.
- [40] E. Asadi, M. Asle Zaeem, The anisotropy of hexagonal close-packed and liquid interface free energy using molecular dynamics simulations based on modified embedded-atom method, Acta Materialia 107 (2016) 337-344.
- [41] Y.-M. Kim, N.J. Kim, B.-J. Lee, Atomistic modeling of pure Mg and Mg–Al systems, Calphad 33(4) (2009) 650-657.
- [42] B.-J. Lee, M.I. Baskes, Second nearest-neighbor modified embedded-atom-method potential, Physical Review B 62(13) (2000) 8564-8567.
- [43] B.-J. Lee, J.-H. Shim, M.I. Baskes, Semiempirical atomic potentials for the fcc metals Cu, Ag, Au, Ni, Pd, Pt, Al, and Pb based on first and second nearest-neighbor modified embedded atom method, Physical Review B 68(14) (2003) 144112.
- [44] B.-J. Lee, M.I. Baskes, H. Kim, Y. Koo Cho, Second nearest-neighbor modified embedded atom method potentials for bcc transition metals, Physical Review B 64(18) (2001) 184102.
- [45] P. Vinet, J.R. Smith, J. Ferrante, J.H. Rose, Temperature effects on the universal equation of state of solids, Physical Review B 35(4) (1987) 1945-1953.
- [46] M.I. Baskes, J.E. Angelo, C.L. Bisson, Atomistic calculations of composite interfaces, Modelling and Simulation in Materials Science and Engineering 2(3A) (1994) 505.
- [47] E. Asadi, M. Asle Zaeem, M.I. Baskes, Phase-field crystal model for Fe connected to MEAM molecular dynamics simulations, JOM 66(3) (2014) 429-436.
- [48] A. Mahata, M. Asle Zaeem, Evolution of solidification defects in deformation of nano-polycrystalline aluminum, Computational Materials Science 163 (2019) 176-185.
- [49] A. Mahata, M. Asle Zaeem, Effects of solidification defects on nanoscale mechanical properties of rapid directionally solidified Al-Cu Alloy: A large scale molecular dynamics study, Journal of Crystal Growth 527 (2019) 125255.
- [50] J.H. Rose, J.R. Smith, F. Guinea, J. Ferrante, Universal features of the equation of state of metals, Physical Review B 29(6) (1984) 2963-2969.
- [51] J.J. Valencia, P. Quested, Thermophysical properties, Modeling for Casting and Solidification Processing 189 (2001).
- [52] J.M. Hughes, M.F. Horstemeyer, R. Carino, N. Sukhija, W.B. Lawrimore, S. Kim, M.I. Baskes, Hierarchical Bridging Between Ab Initio and Atomistic Level Computations: Sensitivity and Uncertainty Analysis for the Modified Embedded-Atom Method (MEAM) Potential (Part B), JOM 67(1) (2015) 148-153.
- [53] M. Horstemeyer, J. Hughes, N. Sukhija, W. Lawrimore, S. Kim, R. Carino, M. Baskes, Hierarchical bridging between ab initio and atomistic level computations: Calibrating the modified embedded atom method (meam) potential (part a), Jom 67(1) (2015) 143-147.
- [54] S. Plimpton, Fast parallel algorithms for short-range molecular dynamics, Journal of computational physics 117(1) (1995) 1-19.

- [55] S. Roy, A. Dutta, N. Chakraborti, A novel method of determining interatomic potential for Al and Al-Li alloys and studying strength of Al-Al3Li interphase using evolutionary algorithms, Computational Materials Science 190 (2021) 110258.
- [56] J. Hughes, M. Horstemeyer, R. Carino, N. Sukhija, W. Lawrimore, S. Kim, M. Baskes, Hierarchical bridging between ab initio and atomistic level computations: Sensitivity and uncertainty analysis for the modified embedded-atom method (meam) potential (part b), Jom 67(1) (2015) 148-153.
- [57] M.-C. Trinh, T. Mukhopadhyay, S.-E. Kim, A semi-analytical stochastic buckling quantification of porous functionally graded plates, Aerospace Science and Technology 105 (2020) 105928.
- [58] M.-C. Trinh, T. Mukhopadhyay, Semi-analytical atomic-level uncertainty quantification for the elastic properties of 2D materials, Materials Today Nano 15 (2021) 100126.
- [59] J.L. Murray, The aluminium-copper system, International metals reviews 30(1) (1985) 211-234.
- [60] V. Vaithyanathan, C. Wolverton, L. Chen, Multiscale modeling of precipitate microstructure evolution, Physical review letters 88(12) (2002) 125503.
- [61] X.Y. Yan, Y.A. Chang, F.Y. Xie, S.L. Chen, F. Zhang, S. Daniel, Calculated phase diagrams of aluminum alloys from binary Al–Cu to multicomponent commercial alloys, Journal of Alloys and Compounds 320(2) (2001) 151-160.
- [62] Y. Grin, F.R. Wagner, M. Armbrüster, M. Kohout, A. Leithe-Jasper, U. Schwarz, U. Wedig, H. Georg von Schnering, CuAl2 revisited: Composition, crystal structure, chemical bonding, compressibility and Raman spectroscopy, Journal of Solid State Chemistry 179(6) (2006) 1707-1719.
- [63] A. Meetsma, J.L. De Boer, S. Van Smaalen, Refinement of the crystal structure of tetragonal Al2Cu, Journal of Solid State Chemistry 83(2) (1989) 370-372.
- [64] C. Wolverton, V. Ozoliņš, Entropically Favored Ordering: The Metallurgy of Al2Cu Revisited, Physical Review Letters 86(24) (2001) 5518-5521.
- [65] W. Zhou, L. Liu, B. Li, Q. Song, P. Wu, Structural, Elastic, and Electronic Properties of Al-Cu Intermetallics from First-Principles Calculations, Journal of Electronic Materials 38(2) (2009) 356-364.
- [66] M.M.a.M. Widom, Alloy database [http://euler.phys.cmu.edu/alloy/], (2009).
- [67] F. Apostol, Y. Mishin, Interatomic potential for the Al-Cu system, Physical Review B 83(5) (2011) 054116.
- [68] C. Wolverton, V. Ozoliņš, Entropically Favored Ordering: The Metallurgy of Al_2Cu Revisited, Physical Review Letters 86(24) (2001) 5518-5521.
- [69] S. Hu, M. Baskes, M. Stan, L. Chen, Atomistic calculations of interfacial energies, nucleus shape and size of θ' precipitates in Al–Cu alloys, Acta materialia 54(18) (2006) 4699-4707.
- [70] V. Vaithyanathan, C. Wolverton, L.Q. Chen, Multiscale Modeling of Precipitate Microstructure Evolution, Physical Review Letters 88(12) (2002) 125503.
- [71] F.R. Eshelman, J.F. Smith, Single-crystal elastic constants of Al2Cu, Journal of Applied Physics 49(6) (1978) 3284-3288.
- [72] C. Ravi, C. Wolverton, V. Ozoliņš, Predicting metastable phase boundaries in Al–Cu alloys from first-principles calculations of free energies: The role of atomic vibrations, EPL (Europhysics Letters) 73(5) (2006) 719.
- [73] D. Nguyen-Manh, D.G. Pettifor, Electronic structure, phase stability and elastic moduli of AB transition metal aluminides, Intermetallics 7(10) (1999) 1095-1106.
- [74] Y.S. Touloukian, Thermal expansion: metallic elements and alloys, Thermophysical properties of matter 12 (1975).
- [75] S.-M. Liang, R. Schmid-Fetzer, Thermodynamic assessment of the Al–Cu–Zn system, part II: Al–Cu binary system, Calphad 51 (2015) 252-260.
- [76] V. Witusiewicz, U. Hecht, S. Fries, S. Rex, The Ag–Al–Cu system: Part I: Reassessment of the constituent binaries on the basis of new experimental data, Journal of alloys and compounds 385(1-2) (2004) 133-143.

- [77] J. Hair, D. Downie, Thermodynamic properties of the Cu-Al system: correlation with bonding mechanisms, Faraday Symposia of the Chemical Society, Royal Society of Chemistry, 1973, pp. 56-63.
- [78] R. Hultgren, P.D. Desai, D.T. Hawkins, M. Gleiser, K.K. Kelley, Selected values of the thermodynamic properties of binary alloys, National Standard Reference Data System, 1973.
- [79] K. Itagaki, A. Yazawa, Heats of Mixing in Liquid Copper or Gold Binary Alloys, Transactions of the Japan Institute of Metals 16(11) (1975) 679-686.
- [80] D.S. Kanibolotsky, O.A. Bieloborodova, N.V. Kotova, V.V. Lisnyak, Thermodynamic properties of liquid Al-Si and Al-Cu alloys, Journal of Thermal Analysis and Calorimetry 70(3) (2002) 975-983.
- [81] V. Sandakov, S. VD, Y. ESIN, P. GELD, HEATS OF FORMATION OF LIQUID COPPER-ALUMINUM ALLOYS, RUSSIAN JOURNAL OF PHYSICAL CHEMISTRY, USSR 45(8) (1971) 1150-&.
- [82] V. Witusiewicz, U.K. Stolz, I. Arpshofen, F. Sommer, Thermodynamics of Liquid Al-Cu-Zr Alloys, Zeitschrift fur Metallkunde 89(10) (1998) 704-713.
- [83] H. Flandorfer, M. Rechchach, A. Elmahfoudi, L. Bencze, A. Popovič, H. Ipser, Enthalpies of mixing of liquid systems for lead free soldering: Al–Cu–Sn system, The Journal of Chemical Thermodynamics 43(11) (2011) 1612-1622.
- [84] W.G. Hoover, Canonical dynamics: Equilibrium phase-space distributions, Physical review A 31(3) (1985) 1695.
- [85] S. Nosé, A unified formulation of the constant temperature molecular dynamics methods, The Journal of chemical physics 81(1) (1984) 511-519.
- [86] B. Predel, H. Landolt, R. Börnstein, Phase equilibria, crystallographic and thermodynamic data of binary alloys, Springer1991.
- [87] A.C. e Silva, J. Ågren, M.T. Clavaguera-Mora, D. Djurovic, T. Gomez-Acebo, B.-J. Lee, Z.-K. Liu, P. Miodownik, H.J. Seifert, Applications of computational thermodynamics—the extension from phase equilibrium to phase transformations and other properties, Calphad 31(1) (2007) 53-74.
- [88] W. Pearson, Lattice spacings and structures of metals and alloys, Vols. I and II (Pergamon Press, Oxford, 1964, 1967) (1958).
- [89] K. Rzyman, Z. Moser, Calorimetric studies of the enthalpies of formation of Al3Ni2, AlNi and AlNi3, Progress in Materials Science 49(3-4) (2004) 581-606.
- [90] S. Kek, C. Rzyman, F. Sommer, Determination of the Enthalpy of Formation of Ternary Ni3Al-Based Alloys, An. Fis. Ser. B 86 (1990) 31-38.
- [91] O. Kubaschewski, W.A. Dench, The heats of formation in the systems titanium-aluminium and titanium-iron, Acta Metallurgica 3(4) (1955) 339-346.
- [92] S. Meschel, O. Kleppa, J. Faulkner, R. Jordan, Metallic alloys: experimental and theoretical perspectives, NATO ASI Series E: Applied Sciences 256 (1994) 103.
- [93] K. Rzyman, Z. Moser, Calorimetric studies of the enthalpies of formation of Al3Ni2, AlNi and AlNi3, Progress in Materials Science 49(3) (2004) 581-606.
- [94] P.A. Korzhavyi, A.V. Ruban, A.Y. Lozovoi, Y.K. Vekilov, I. Abrikosov, B. Johansson, Constitutional and thermal point defects in B 2 NiAl, Physical Review B 61(9) (2000) 6003.
- [95] O. Kubaschewski, The heats of formation in the system aluminium + nickel + titanium, Transactions of the Faraday Society 54(0) (1958) 814-820.
- [96] A. Pasturel, C. Colinet, A.T. Paxton, M.v. Schilfgaarde, First-principles determination of the Ni-Al phase diagram, Journal of Physics: Condensed Matter 4(4) (1992) 945-959.
- [97] A. Kumar, A. Chernatynskiy, T. Liang, K. Choudhary, M.J. Noordhoek, Y.-T. Cheng, S.R. Phillpot, S.B. Sinnott, Charge optimized many-body (COMB) potential for dynamical simulation of Ni–Al phases, Journal of Physics: Condensed Matter 27(33) (2015) 336302.
- [98] G. Simmons, H. Wang, Single crystal elastic constants and calculated aggregate properties, (1971).
- [99] G. Simmons, Single crystal elastic constants and calculated aggregate properties, Southern Methodist Univ Dallas Tex, 1965.

- [100] D. Shi, B. Wen, R. Melnik, S. Yao, T. Li, First-principles studies of Al–Ni intermetallic compounds, Journal of Solid State Chemistry 182(10) (2009) 2664-2669.
- [101] Y.-K. Kim, H.-K. Kim, W.-S. Jung, B.-J. Lee, Development and application of Ni-Ti and Ni-Al-Ti 2NN-MEAM interatomic potentials for Ni-base superalloys, Computational Materials Science 139 (2017) 225-233.
- [102] A. Jain, S.P. Ong, G. Hautier, W. Chen, W.D. Richards, S. Dacek, S. Cholia, D. Gunter, D. Skinner, G. Ceder, K.A. Persson, Commentary: The Materials Project: A materials genome approach to accelerating materials innovation, APL Materials 1(1) (2013) 011002.
- [103] R.E. Watson, M. Weinert, Transition-metal aluminide formation: Ti, V, Fe, and Ni aluminides, Physical Review B 58(10) (1998) 5981-5988.
- [104] K. Rzyman, Z. Moser, R. Watson, M. Weinert, Enthalpies of formation of Ni 3 Al: Experiment versus theory, Journal of phase equilibria 17(3) (1996) 173-178.
- [105] I. Ansara, N. Dupin, H.L. Lukas, B. Sundman, Thermodynamic assessment of the Al®Ni system, Journal of Alloys and Compounds 247(1) (1997) 20-30.
- [106] E.-T.H.a.H.L. Luke, Z. Mrtulltie 66 (1975) 98.
- [107] F.R. De Boer, W. Mattens, R. Boom, A. Miedema, A. Niessen, Cohesion in metals, (1988).
- [108] K. Rzyman, Z. Moser, R.E. Watson, M. Weinert, Enthalpies of formation of AlNi: Experiment versus theory, Journal of Phase Equilibria 19(2) (1998) 106.
- [109] P. Nash, O. Kleppa, Composition dependence of the enthalpies of formation of NiAl, Journal of Alloys and Compounds 321(2) (2001) 228-231.
- [110] A. Fourdeux, P. Lesbats, Annealing out of quenched-in vacancies in an ordered B2 type Fe-Al single crystal, Philosophical Magazine A 45(1) (1982) 81-93.
- [111] N. Junqua, J. Desoyer, P. Moine, Electron microscopy observation of quenching defects in an ordered alloy of B2 type: Fe–40 at% Al, Physica status solidi (a) 18(1) (1973) 387-395.
- [112] M. Mendiratta, C. Law, Dislocation energies and mobilities in B2-ordered Fe-Al alloys, Journal of materials science 22(2) (1987) 607-611.
- [113] C. Vailhé, D. Farkas, Shear faults and dislocation core structure simulations in B2 FeAl, Acta Materialia 45(11) (1997) 4463-4473.
- [114] E. Lee, B.-J. Lee, Modified embedded-atom method interatomic potential for the Fe–Al system, Journal of Physics: Condensed Matter 22(17) (2010) 175702.
- [115] G.P. Das, B.K. Rao, P. Jena, S.C. Deevi, Electronic structure of substoichiometric Fe-Al intermetallics, Physical Review B 66(18) (2002) 184203.
- [116] D. Connétable, P. Maugis, First principle calculations of the κ -Fe3AlC perovskite and iron–aluminium intermetallics, Intermetallics 16(3) (2008) 345-352.
- [117] F. Lechermann, M. Fähnle, J.M. Sanchez, First-principles investigation of the Ni–Fe–Al system, Intermetallics 13(10) (2005) 1096-1109.
- [118] L. Shaojun, D. Suqing, M. Benkun, First-principles calculation of vibrational entropy for Fe-Al compounds, Physical Review B 58(15) (1998) 9705-9709.
- [119] N. Sodré, P. Guillermo Gonzales-Ormeño, H.M. Petrilli, C.G. Schön, Ab initio calculation of the BCC Fe–Al–Mo (Iron–Aluminum–Molybdenum) phase diagram: Implications for the nature of the $\tau 2$ phase, Calphad 33(3) (2009) 576-583.
- [120] A. Kellou, T. Grosdidier, J.M. Raulot, H. Aourag, Atomistic study of magnetism effect on structural stability in Fe3Al and Fe3AlX (X = H, B, C, N, O) alloys, physica status solidi (b) 245(4) (2008) 750-755.
- [121] C.J. Smithells, E.A. Brandes, Smithells metals reference book, 1992.
- [122] P. Maugis, J. Lacaze, R. Besson, J. Morillo, Ab Initio calculations of phase stabilities in the Fe–Al–C system and CALPHAD-Type assessment of the iron-rich corner, Metallurgical and Materials Transactions A 37(12) (2006) 3397-3401.

- [123] P.G. Gonzales-Ormeño, H.M. Petrilli, C.G. Schön, Ab-initio calculations of the formation energies of BCC-based superlattices in the Fe[®]Al system, Calphad 26(4) (2002) 573-582.
- [124] P.D. Desai, Thermodynamic Properties of Selected Binary Aluminum Alloy Systems, Journal of Physical and Chemical Reference Data 16(1) (1987) 109-124.
- [125] M. Friák, J. Neugebauer, Ab initio study of the anomalous volume-composition dependence in Fe–Al alloys, Intermetallics 18(7) (2010) 1316-1321.
- [126] C.L. Fu, M.H. Yoo, Deformation behavior of B2 type aluminides: FeAl and NiAl, Acta Metallurgica et Materialia 40(4) (1992) 703-711.
- [127] J. Breuer, A. Grün, F. Sommer, E. Mittemeijer, Enthalpy of formation of B2-Fe 1- x Al x and B2-(Ni, Fe) 1- x Al x, Metallurgical and Materials Transactions B 32(5) (2001) 913-918.
- [128] J. Elliott, F. Woolley, Heats of solution of aluminum, copper, and silicon in liquid iron, Trans Metall Soc AIME 239(12) (1967) 1872-1883.
- [129] M. Petrushevsky, Y. Esin, P. Geld, V. Sandakov, Concentration Dependence of the Enthalpy of Formation of Molten Fe-Al Alloys, Izvest. Akad. Nauk SSSR Metally (6) (1972) 193-197.
- [130] H.-D. Dannöhl, Kalorimetrische Bestimmung der Bildungsenthalpien einiger intermetallischer Phasen, Verlag nicht ermittelbar, 1971.